

Video Classification With CNNs: Using The Codec As A Spatio-Temporal Activity Sensor

Aaron Chadha, Alhabib Abbas and Yiannis Andreopoulos, *Senior Member, IEEE*

Abstract—We investigate video classification via a two-stream convolutional neural network (CNN) design that directly ingests information extracted from compressed video bitstreams. Our approach begins with the observation that all modern video codecs divide the input frames into macroblocks (MBs). We demonstrate that selective access to MB motion vector (MV) information within compressed video bitstreams can also provide for selective, motion-adaptive, MB pixel decoding (a.k.a., MB texture decoding). This in turn allows for the derivation of spatio-temporal video activity regions at extremely high speed in comparison to conventional full-frame decoding followed by optical flow estimation. In order to evaluate the accuracy of a video classification framework based on such activity data, we independently train two CNN architectures on MB texture and MV correspondences and then fuse their scores to derive the final classification of each test video. Evaluation on two standard datasets shows that the proposed approach is competitive to the best two-stream video classification approaches found in the literature. At the same time: (i) a CPU-based realization of our MV extraction is over 977 times faster than GPU-based optical flow methods; (ii) selective decoding is up to 12 times faster than full-frame decoding; (iii) our proposed spatial and temporal CNNs perform inference at 5 to 49 times lower cloud computing cost than the fastest methods from the literature.

Index Terms—video coding, classification, deep learning.

I. INTRODUCTION

FOR THE last 50 years, the holy grail of machine learning with visual data has been to translate *pixels to concepts* [1], e.g., classify a pixel-domain video sequence according to its contents (tennis match, horror film, cooking show, people marching,...). However, it has been argued recently [2], [3] that that there is no strong scientific basis for this focus on pixels: it simply stems from the 140-year old legacy of video being displayed as sequences of still frames comprising the raster-scan of picture elements. Pixel-domain video representations are in fact known to be cumbersome for cognitive video analysis, primarily due to two aspects: (i) all state-of-the-art methods for high-level semantic description in video require memory- and compute-intensive decoding and pixel-domain processing, such as optical flow calculations [4]–[6]; (ii) the

high resolution & high frame-rate nature of decoded video and the format inflation (from standard to super-high definition, 3D, multiview, etc.) require highly-complex convolutional neural networks (CNNs) that impose massive computation and storage requirements [7].

Inspired by these observations, hardware designs of neuromorphic sensors, a.k.a., silicon retinas [2], [3], have been proposed recently. Unlike conventional active pixel sensors, silicon retinas create a spatio-temporal activity representation (a.k.a., spatio-temporal spike event stream) representing the illumination changes caused by object motion, while incurring very low power and low latency. Nevertheless, due to the need to be compliant to display technology, pixels and video frames are here to stay: after all, pixel-based video frames are being used today within all conversational, entertainment and mainstream visual surveillance services. However, because of storage and data-transfer limitations, all camera chipsets and video processing pipelines provide compressed-domain video formats like MPEG/ITU-T AVC/H.264 [8] and HEVC [9], or open-source video formats like VP9 [10] and AOMedia Video 1 instead of uncompressed (pixel-domain) video. Alas, the state-of-the-art in CNN-based classification and recognition in video [4]–[6] ignores the fact that video codecs can be tuned at the macroblock (MB) level. For example, the MPEG/ITU-T AVC/H.264 and HEVC codecs divide the input video frames into 16×16 pixel MBs that form the basis for the adaptive inter (and intra) prediction. Inter-predicted MBs are (optionally) further partitioned into blocks that are predicted via motion vectors (MVs) that represent the displacement from matching blocks in previous or subsequent frames.

The research hypothesis of this paper is to consider the video encoder as an imperfect-yet-highly-efficient “sensor” that derives spatio-temporal activity representations with minimal processing. With regards to the temporal activity, we demonstrate that we can obtain MV representations from the compressed bitstream that are highly correlated with optical flow estimates. We then propose a three-dimensional CNN that directly leverages on such MB MV information and compensates for the sparsity of these MB MVs with larger temporal extents. With regards to the spatial activity, we show that selective MB texture decoding can take place based on thresholding of the MB MV information. By superimposing such selectively-decoded MB texture information on sparsely-decoded frames, we obtain spatial representations that are shown to be visually similar to the corresponding fully-decoded video frames. This allows for the parsimonious use of a spatial CNN to augment the classification results derived from the temporal stream. Our results with the fusion of

AC and AA are with the Electronic and Electrical Engineering Department, University College London, Roberts Building, Torrington Place, London, WC1E 7JE, UK (e-mail: {aaron.chadha.14, alhabib.abbas.13}@ucl.ac.uk). YA is with the Electronic and Electrical Engineering Department, University College London, Roberts Building, Torrington Place, London, WC1E 7JE, UK, and also with Dithen, 843 Finchley Road, London, NW11 8NA, UK, www.dithen.com (e-mail: i.andreopoulos@dithen.com). We acknowledge support from: EPSRC (project EP/P02243X/1), Innovate UK (project DELVE-VIDEO 132739), The Leverhulme Trust (RAEng/Leverhulme Senior Research Fellowship of Y. Andreopoulos) and the Royal Commission for the Exhibition of 1851 (Fellowship of A. Chadha). This work has been presented in part at the 2017 IEEE International Conference on Image Processing, Beijing, China.

this two-stream CNN design on two widely-used datasets show that competitive accuracy is obtained against the state-of-the-art, with extraction and classification complexity that is found to be one to three orders-of-magnitude lower than that of all previous approaches based on pixel-domain video. Importantly, the complexity gains from using compressed MB bitstreams are future-proof: as video, multi-view and 3D video format resolutions and frame rates increase to accommodate advances in display technologies, the gains provided by such approaches will increase commensurably to the change in spatio-temporal sampling. This paves the way for exabyte-scale video datasets to be newly-discovered and analysed over commodity hardware.

II. RELATED WORK

Due to their outstanding performance in image classification [11], deep convolutional neural networks (CNNs) have recently come to the forefront in video classification, remaining competitive to or surpassing performance of traditional methods derived on hand-crafted features, such as improved dense trajectories (IDT) [12], [13]. With increasing dataset sizes and complexity in classification and retrieval, deep and scalable CNN architectures are capable of learning more complex representations. Karpathy *et al.* [14] proposed extending the CNN architecture from image to video by performing spatio-temporal convolutions in the first convolutional layers over a 4D video chunk $V \in \mathbb{R}^{W \times H \times K \times T}$, where W, H are the spatial dimensions, K is the number of channels and T is the number of frames in the chunk. This is the premise behind their slow-fusion architecture, which uses 3D convolutions on RGB frame chunks in the first 3 layers, thus encompassing the full spatio-temporal extent of the input. Tran *et al.* [15] attempted to improve accuracy by using a deep 3D CNN architecture (resembling VGGnet [16]) together with spatio-temporal convolutions and pooling in all layers, albeit with heavy computational cost. In this paper, we show that a deeper 2D CNN architecture ingesting a single RGB frame should be sufficient to perform competitively to 3D architectures, whilst providing simplicity in training and pre-processing the inputs.

Indeed, Simonyan *et al.* [4], argue that the problem is not the depth or spatio-temporal extent of the architecture but rather the nature of the RGB input that does not effectively present motion information to the CNN. They propose using a 2D architecture with dense optical flow to represent the temporal component of the video. Notably, this temporal CNN is shown to outperform an equivalent 2D spatial stream ingesting RGB frames. Performance can be improved further by fusing the temporal and spatial streams using a simple score averaging. This two stream architecture achieves 88.0% on UCF-101. Nevertheless, the computational cost remains high due to the requirement to extract Brox optical flow [17] for the temporal stream. In this paper, we also employ a two stream architecture to model the temporal motion and scene information independently. In order to reduce the computational overhead from having to fully decode and process the video, we circumvent the highly-complex optical flow calculation by using MV representations extracted directly from the video codec.

Recent work [18] has used hand-crafted features, in the form of a spatio-temporal Bag-of-Words approach on refined MV representations for object-based segmentation in video. The use of codec MV representations has also been proposed for action recognition by Kantorov and Laptev [19]. However, their approach uses Fisher vectors, which achieves lower accuracy in standard action recognition datasets. Recently, Zhang *et al.* [6] utilized codec MVs as an input to a 2D CNN in their action recognition, termed EMV-CNN, but their framework requires optical-flow based training (in their proposed teacher net). This constrains the training to relatively small volumes of video content and requires upsampled P and B-frame MV fields during inference due to the teacher-student supervision transfer [6]. Our paper is the first to achieve state-of-the-art performance *without* the use of optical flow and with substantially higher speed in comparison to EMV-CNN and all existing alternatives. In addition, given that the spatial stream predominantly learns on scene information that tends to be persistent across frames, we gain by sparse frame decoding combined with motion adaptive superpositioning of decoded MB texture information to generate intermediate frames at a finer temporal resolution¹.

One of the main issues with the related work described above is the short temporal extent of the inputs [21], [22]; each input is a small group of frames that only encapsulates a second or so of the video. This does not account for cases where temporal dependencies extend over longer durations. Feichtenhofer *et al.* [23] attempted to resolve this issue by using multiple copies of their two stream network. The copies are spread over a coarse temporal scale, thus encompassing both coarse and fine motion information with an optical flow input. The architecture is spatially and then temporally fused using a 3D convolution and pooling. Despite achieving state-of-the-art results on UCF-101 and HMDB-51 datasets, this approach requires very computationally demanding processing for both training and testing. This is in part due to the joint training, which can cause a parameter explosion depending on the chosen architecture and fusion method (see Table 1 of Feichtenhofer *et al.* [23]). Alternatively, Laptev *et al.* [5] argue that increasing the temporal extent is simply a case of taking the optical flow component over a larger temporal extent. In order to minimize the complexity of the network, they downsize the frames, thus reducing the spatial dimensions. Combining their two stream architecture with improved dense trajectories yields 92.7% on UCF-101. Finally, Action VLAD [24] was proposed as the means to encompass a longer temporal extent by pooling features spatio-temporally into a VLAD descriptor. However, this aggregation requires (i) additional VLAD pre-processing computation and (ii) multiple CNN copies during training in order to cover the entire temporal extent of the video. These requirements raise significant demands in GPU memory and CPU preprocessing capability. Contrary to these proposals, our temporal stream input (as extracted from the video codec), is inherently of low spatial resolution, thus

¹While initial results with the proposed MV-based CNN approach have been presented in our corresponding conference paper [20], MV-based selective MB texture decoding and the fusion of the temporal 3D-CNN with a spatial CNN are proposed here for the first time.

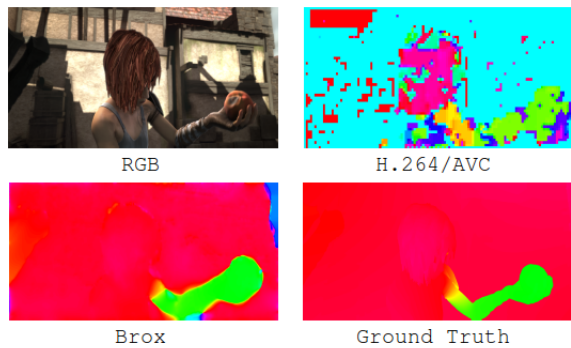


Fig. 1: RGB frame from the MPI-Sintel dataset and pseudocolored images of the motion information amplitude. The H.264/AVC MB motion vectors are correlated with Brox optical flow extracted from decoded video frames [17] [25] and the ground-truth motion available for this synthetic video.

allowing for significantly lower complexity in processing. This enables us to feed an even larger temporal extent into our 3D CNN. We also improve the architecture by minimizing the number of activations in the lower layers with a temporal downsizing (using a stride of 2); this allows us to reduce the bottleneck in processing the temporal input volume.

Another method of generating CNNs with a long temporal extent is to integrate a recursive neural network (RNN) into the architecture. In principle, an RNN provides for infinite temporal context up to the present frame. Donahue *et al.* [26] use a 2D CNN to extract features from individual frames. These are subsequently fed into a stack of long short term memory (LSTM) networks for sequence learning over the input. Due to parameter sharing over time, this model scales to arbitrary sequence lengths. Ng *et al.* [27] extend this by considering the effects of appending the CNN with feature pooling versus an LSTM, prior to class fusion. Their results demonstrate that pooling is a good alternative to using an LSTM and achieves competitive accuracy (88.2% vs 88.6% on UCF-101). They also note that simply appending a 2D CNN with an LSTM stack has its limitations. For one, the LSTM is likely to only focus on global temporal motion, such as shot detection and not the fine temporal cues inherent in groups of consecutive frames. In this paper, we decide against integrating LSTMs into our framework as our temporal extent is sufficiently large to encompass the entire video duration.

III. SELECTIVE MB MOTION VECTOR DECODING

Video compression standards like MPEG/ITU-T AVC/H.264, and HEVC rely on motion estimation and compensation as their main method to decorrelate successive input frames. Macroblock motion vectors are derived by temporal block matching and can be interpreted as approximations of the underlying optical flow [28] [19], as shown in the example of Fig. 1.

To derive a temporal activity map from encoded motion compensation parameters, we apply the following steps:

- 1) Motion vectors are extracted from certain compressed MB information of the utilized video codec².
- 2) If necessary, motion vectors are interpolated spatially to generate a finer representation of motion activity in the video, i.e., with resolution corresponding to 8×8 or 4×4 blocks, and also to “fill in” for macroblocks where the video encoder may have used an intra prediction mode.

For the spatial stream, we employ selectively-decoded MB texture information using the extracted MVs as activity indicators. We do this by decoding one frame every X frames, with X set to inf , indicating that only the first frame of the video is decoded. In between fully-decoded frames, “rendered” frames can be produced at frame interval R , with $1 \leq R \leq X$. Each rendered frame is initialized as a copy of the immediately preceding fully-decoded frame. Then, texture information at active MB positions is decoded and replaces the initialized values in the corresponding locations in the rendered frame. Two examples of this process are shown in Fig. 2. We consider the area within a macroblock to be active when the corresponding MV information exceeds a specified threshold A , $A \geq 0$. As an illustration, Fig. 3 shows a grayscale activity map derived from the MVs of Fig. 2(b). To achieve such blockwise selective MB texture decoding via the `libavcodec` library [29], we use the motion vectors from `AVMotionVector` to access `AVFrame::data` and write decoded MB texture data wherever the conditions specified by $\{X, R, A\}$ are met. By increasing the values for $\{X, R, A\}$ we can decrease the frequency of full decoding and selective MB texture decoding in order to achieve any extraction speed desired within a practical application context. In addition, even though it is not explored in this paper, we can investigate adaptive control of $\{X, R, A\}$ based on the average MV activity level within each video sequence.

IV. PROPOSED FRAMEWORK FOR COMPRESSED-DOMAIN CLASSIFICATION

In this section we describe the proposed framework for training a temporal stream of MB motion vectors extracted directly from the video bitstream and a spatial stream comprising selective (motion-dependent) MB RGB texture decoding, and consider how the two streams can be fused during testing.

A. Network Input

1) *Temporal Stream:* For our temporal stream input, we extract and retain only P-type MB MVs, i.e., uni-directionally predicted MBs [8], [9]. The standard UCF-101 [30] and HMDB-51 [31] datasets are composed of 320×240 RGB

²Based on FFmpeg’s widely-used `libavcodec` library (which supports most MPEG/ITU-T standards) [29], we make use of the `AVMotionVector` structure (declared within the `avutil.h` header file) as explained in the following. When `libavcodec` attempts to read the compressed bitstream of a video frame using the `av_read_frame()` function, our MB MV extractor calls the `av_frame_get_side_data()` function to extract the MV parameters and place them in the `AVMotionVector` structure. Once the file parsing is completed, the horizontal and vertical coordinates of MVs of each MB within this structure are written in 16-bit integer binary format to disk in order to be used by the proposed 3D CNN. By limiting the bitstream access to solely using this function for the MB MVs, one can achieve the speed gains reported in Section V.

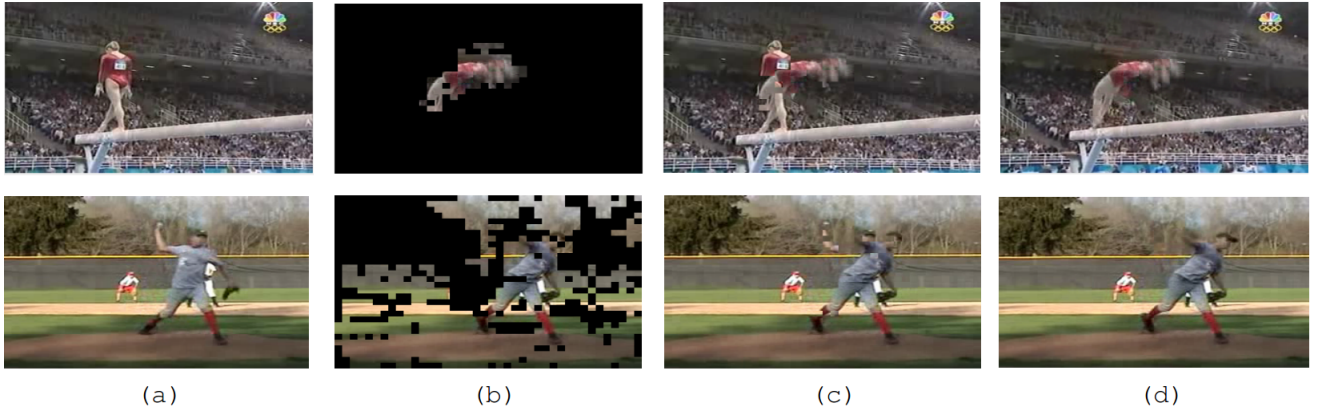


Fig. 2: Two scenes from UCF-101 with & without camera motion (top & bottom row respectively); (a) Reference frame; (b) Selective decoding of MB texture ($A = 0$); (c) Rendered frame; (d) Fully decoded frame corresponding to the rendered frame.

pixels per frame. Therefore, for a frame comprising P-type MBs, a block size of 8×8 pixels results in a motion vector field $\Phi_T \in \mathbb{R}^{W_T \times H_T \times K_T}$ of dimension $40 \times 30 \times 2$, where $W_T \times H_T$ is the motion vector spatial resolution and the number of channels $K_T = 2$ refers to the δx and δy motion vector components.

In order to compensate for the low spatial resolution $W_T \times H_T$, we take a long temporal extent of motion vectors over $T > 100$ consecutive P frames. This is contrary to recent proposals based on high-resolution optical flow [4], [14], which typically ingest only a few frames per input (typically around 10). This is because, even with the latest GPU hardware, a long temporal extent cannot be processed without sacrificing the spatial resolution of the optical flow [4], [14]. On the other hand, given that our MB motion vector input is inherently low-resolution, it is amenable to a longer temporal extent, which is more likely to include the entirety of relevant action that is essential for the correct classification of the video. For example, we have found that the accuracy increases greatly for UCF-101 evaluated on our 3D CNN when moving from 10 to 100 frames, but eventually plateaus when T becomes sufficiently large such that the input extends to almost all P-type frames of the video files of the dataset. Therefore, we fix the temporal extent T to 160, which is roughly the average number of P-frames per video in UCF-101.

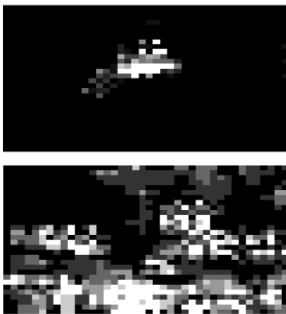


Fig. 3: MV activity maps corresponding to Fig. 2(b).

In order to make our network input independent of the

video resolution, we use a fixed spatial size $N_T \times N_T$ which is cropped/resized from Φ_T . In this paper, we set $N_T = 24$, which is large enough to encompass the action region without compromising accuracy, whilst allowing for data augmentation via random cropping. Furthermore, given it is divisible by eight, the P-frames can be continuously downsampled by a factor of 2 with pooling layers, without requiring any padding. Our final network input $\hat{\Phi}_T \in \mathbb{R}^{N_T \times N_T \times K_T \times T}$ is thus 4D and can be ingested by a 3D CNN. As exemplified in numerous works [14], [15], the advantage of using a 3D CNN architecture with a 4D input, versus stacking the frames as channels and using a 3D input of size $N_T \times N_T \times TK_T$ with a 2D CNN, is that, rather than collapsing to a 2D slice when convolving within the CNN, we preserve the temporal structure during filtering.

2) *Spatial Stream*: Previous work has shown that stacking RGB frames channel-wise and ingesting such volumes into a 2D CNN does not necessarily improve performance [4], [14]. Indeed, one option is to train a deep 3D CNN on a 4D RGB frame input, which is the proposed configuration for our temporal stream (with MV inputs). Whilst this has been shown to improve performance with RGB frames [15], it is far more computationally expensive to implement when the inputs are at pixel resolution, i.e., typically 224×224 for CNNs trained on ImageNet [32]. Therefore, the complexity of the network in terms of activations and weights quickly becomes unmanageable.

Our approach alleviates these problems by simply ingesting single RGB frames from the video as inputs to a 2D CNN, in order to exclusively model the scene semantics in the image; these comprise geometry, color and background information that can not be extracted from the P-frames directly. For example, in the case of action recognition, the green grass and net and racket texture patterns in the frame could distinguish a sequence as being related to tennis, rather than swimming. Given that such spatial structures and color information tends to be persistent across frames belonging to the same type of scene, we can gain substantial storage and complexity savings by our proposed sparse full-frame decoding and selective superpositioning of MB RGB texture decoding according to



Fig. 4: 3D CNN architecture: the blue, orange and yellow blocks represent convolutional, pooling and fully-connected layers; F is the filter size for the convolutional layers (or window size for pooling), formatted as width \times height \times time; S is the filter/window stride; D is the number of filters (or number of hidden units) for the convolutional and fully-connected layers.

the motion activity, as described in Section III and illustrated in Fig. 2 and Fig. 3.

In order to make our input independent of the video resolution, we follow the approach of Simonyan *et al.* [4]. That is, we first resize the RGB frame, such that the smaller side is equal to 256 and we keep the aspect ratio. From the resized frame $\Phi_S \in \mathbb{R}^{W_S \times H_S \times K_S}$, we crop/resize a fixed spatial size $N_S \times N_S$; $N_S = 224$. Our spatial stream input is thus of size $224 \times 224 \times 3$.

B. Network Architecture

Our 3D CNN architecture is illustrated in Fig. 4. All convolutions and pooling are spatiotemporal in their extent. 3D pooling is performed over a $2 \times 2 \times 2$ window with spatiotemporal stride of 2. The first two convolutional layers use 3D filters of size $3 \times 3 \times 3$ to learn spatiotemporal features. With a $24 \times 24 \times 2 \times 160$ motion vector input, the third convolutional layer receives input of size $6 \times 6 \times 2 \times 10$. Therefore, we set the filter size of the third, fourth and fifth convolutional layers to $2 \times 2 \times 2$, as this is sufficiently large to encompass the spatial extent of the input over the three layers whilst minimizing the number of parameters. In order to maintain efficiency when training/evaluating, we also use a temporal stride of 2 in the first and second convolutional layers to quickly downsize the motion vector input; in all other cases we set the stride to 1 for convolutional layers. The temporal downsizing substantially minimizes the number of activations (and thus, the number of floating point operations) in the lower layers. All convolutional layers and the FC6 & FC7 layers use the parametric ReLU activation function [33].

It is important to note that our network has substantially less parameters and activations than other architectures using optical flow. In particular, our 3D CNN stores 29.4 million weights. For comparison, ClarifaiNet [34] and similar configurations that are commonly used for optical-flow based classification [4], [6] require roughly 100 million parameters.

For the spatial stream, we opt for the commonly used VGG-16 [16] architecture, as it is sufficiently deep to learn complex representations from the input frames. The CNN is typically trained on ImageNet [32] for image classification. While we have also obtained similar results with shallower networks, VGG-16 allows for better generalization to larger datasets.

C. Network Training

We train on the temporal and spatial streams independently, as this permits sequential training on a single GPU and simplifies management of resources such as GPU RAM. It additionally permits evaluation on a single stream for faster runtime. The training details for each stream are as follows.

1) *Temporal Stream*: We train the temporal stream using stochastic gradient descent with momentum set to 0.9. The initialization of He *et al.* [33] is extended to 3D and the network weights are initialized from a normal distribution with variance inversely proportional to the fan-in of the filter inputs. Mini-batches of size 64 are generated by randomly selecting 64 training videos. From each of these training videos, we choose a random index from which to start extracting the P-frame MB motion vectors. From this position, we simply loop over the P-type MBs in temporal order until we extract motion vectors over T consecutive P frames. This addresses the issue of videos having less than T total P frames, e.g., cases where the video is only a few seconds long. For UCF-101, we train from scratch; the learning rate is initially set to 10^{-2} and is decreased by a factor of 0.1 every 30k iterations. The training is completed after 70k iterations. Conversely, for HMDB-51, we compensate for the small training split by initializing the network with pre-trained weights from UCF-101 (split 1). The learning rate is initialized at 10^{-3} and decayed by a factor of 0.1 every 15k iterations, for 30k iterations.

To minimize the chance of overfitting due to the low spatial resolution of these motion vector frames and the small size of the training split for both UCF-101 and HMDB-51, we supplement the training with heavy data augmentation. To this end, we concatenate the motion vectors into a single $W_T \times H_T \times 2T$ volume and apply the following steps; (i) a multi-scale random cropping to fixed size $N_c \times N_c \times 2T$ from this volume, by randomly selecting a value for N_c from $N_T \times c$ with $c \in \{0.5, 0.667, 0.833, 1.0\}$; as such, the cropped volume is randomly flipped and spatially resized to $N_T \times N_T \times 2T$; (ii) zero-centering the volume by subtracting the mean motion vector value from each motion vector field Φ_T , in order to remove possible bias; the δx and δy motion vector components can now be split into separate channels, thus generating our 4D network input $\hat{\Phi}_T$. During training, we additionally regularize the network by using dropout ratio of 0.8 on the FC6 and FC7 layers together with weight decay of 0.005.

2) *Spatial Stream*: We also train the spatial stream independently using stochastic gradient descent with momentum set to 0.9. As with the temporal stream, mini-batches of 64 are amalgamated over 64 randomly selected videos. We take advantage of the transferability of features from image to video classification, and pretrain all layers of our VGG-16 architecture on ILSVRC'12 [11]; all layers are subsequently fine-tuned on the video training sets. The learning rate is initialized at 10^{-3} and decayed by a factor of 0.1. We complete training at 15k iterations.

Again, due to the small training sizes, we risk overfitting during training; therefore we set dropout and weight decay

on the first two fully connected layers to 0.8 and 0.005 respectively. We also use a multi-scale random cropping of the resized RGB frame by randomly selecting a value from $N_S \times d$ with $d \in \{0.857, 1.0, 1.143\}$; the cropped volume is subsequently randomly flipped, spatially resized to $N_S \times N_S \times 3$ and zero-centered as per the temporal stream.

D. Testing

During testing, per video, we generate 2 volumes of temporal size T from which to evaluate on the temporal stream. The starting indices for the volumes are at the first P-frame and at half the total number of P-frames. Per volume, we crop the four corners, the center of the image (and its mirror image) to size $N_T \times N_T \times 2 \times T$. In order to generate our prediction for the video, we take the maximum score over all crops. Due to the low resolution and short duration of the HMDB-51 and UCF-101 videos, taking these extra crops and volumes is often redundant as the spatial resolution of the P-frames is low and the temporal extent T of the input is large enough to encompass the entire video duration. However, our approach is better suited to videos “in the wild” and we can afford the use of extra crops due to the low complexity of our 3D CNN.

We evaluate on the spatial stream by extracting only 5 frames from the set per video, albeit with only a single center crop (and its horizontal flip) of size $N_S \times N_S \times 3$. In our experiments, we have found this to be sufficient for the case of trimmed action recognition, where most frames are relevant to the associated video label. The frames are extracted at evenly spaced intervals from the video. To generate our prediction, we again compute the maximum score over all extracted frames. In order to produce a final score for the fusion of the two modalities, we simply average their maximum scores, which is equivalent to combining knowledge from the most relevant input in each stream.

V. EXPERIMENTAL RESULTS

A. End-Point Error and Speed of MB MV Extraction and Decoding vs. Optical Flow Methods used in Video Classification

In order to examine the accuracy and extraction time of our approach versus decoding and optical flow estimation, we perform a comparison against the Brox [35] and FlowNet2 [25] optical flow estimation methods that were respectively used (amongst others) by Simonyan *et al.* [4] and Brox *et al.* [25]. Table I presents the motion field estimation accuracy, measured in terms of end-point error (EPE) on MPI-Sintel, for which ground truth motion flow is also available (see Fig. 1). Since our CNN architecture downsamples the optical flow before ingestion [4], we measure the EPE for our MV flow estimation at the resolution of our CNN input. Under these settings, Table I shows that the EPE of our approach is 1.75 to 4.86 times higher than that of optical flow methods. Despite the detrimental accuracy, our EPE results remain low enough to indicate high correlation with the ground-truth motion flow and the optical-flow based methods. Indeed, the results presented in the following subsections show that the codec MB MV accuracy suffices for classification results that are competitive to the state of the art.

TABLE I: Motion field end-point error (EPE) for the proposed approach, Brox [35] and FlowNet2 [25].

Input	EPE
Proposed, MV	15.26
Brox	8.70
FlowNet2	3.14

TABLE II: Flow estimation and decoding speed results for the proposed approach, Brox [35] and FlowNet2 [25].

Input	Frames Per Second (FPS)	
	Flow Estimation	Decoding
Proposed, $X = 10$	18226 (CPU)	1180 (CPU)
Proposed, $X = 50$	18226 (CPU)	2016 (CPU)
Brox	18.64 (GPU)	168 (CPU)
FlowNet2	12.08 (GPU)	168 (CPU)

In order to measure flow estimation and decoding speed (with I/O) in terms of frames per second (FPS), we now use video content that corresponds to our video classification tests, i.e., 100 video sequences from UCF-101 (see next subsection for the details of this dataset). All CPU-based experiments were carried out on an Amazon Web Services (AWS) EC2 r3.xlarge instance (Intel Xeon E5-2670 v2 CPU), while all GPU-based experiments were carried out on a AWS EC2 p2.xlarge instance (Tesla K80 GPU). For our selective decoding approach described in Section III, we select values for the decoding interval X that correspond to the settings used in our video classification tests. The results of this experiment are summarised in Table II. In terms of flow estimation speed, our CPU-based MV flow extraction is more than 1500 times faster than FlowNet2 and more than 977 times faster than Brox flow (both running on a GPU), as it does not require video decoding or any optical flow computation. At current AWS pricing³, GPU instances require more than 2.7 times the cost of CPU instances; as such, our AWS-based implementation has more than 2600 times lower cost. This means that, for the public cloud cost that an optical flow method will process 1 hour of video, our approach will be able to process more than three and a half months of video footage.

In terms of decoding speed, Table II shows that selective decoding is an order of magnitude faster than the full-frame decoding required for Brox and FlowNet2. We illustrate the influence of selective decoding on the achieved FPS in more detail in Fig. 5. The results show that the decoding FPS increases rapidly until $X > 50$ and begins to saturate after this point. In order to associate this speed up with a measure for the expected visual quality of the selective decoding and rendering approach, we plot the average structural similarity index (SSIM) [36] for multiple values of X in Fig. 6, using the fully-decoded video sequences as reference. By combining the two figures, it is evident that, as the decoding speed increases and reaches a saturation at around 2500 FPS, the quality of all rendered frames decreases and plateaus at SSIM values around 0.85. We next assess whether the motion flow accuracy and

³AWS EC2 spot pricing, (r3.xlarge vs. p2.xlarge N. Virginia, Sept. 2017)

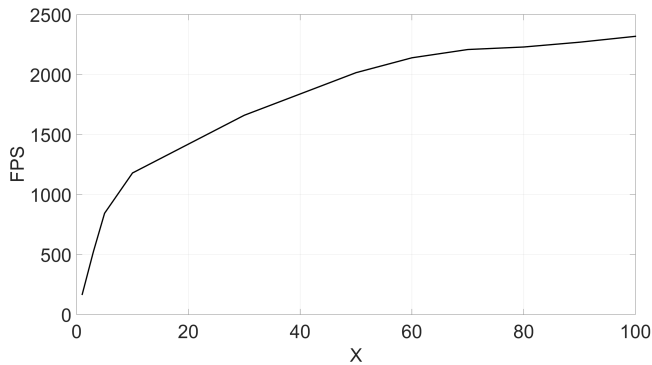


Fig. 5: Achieved FPS of selective decoding for varying decoding interval X .

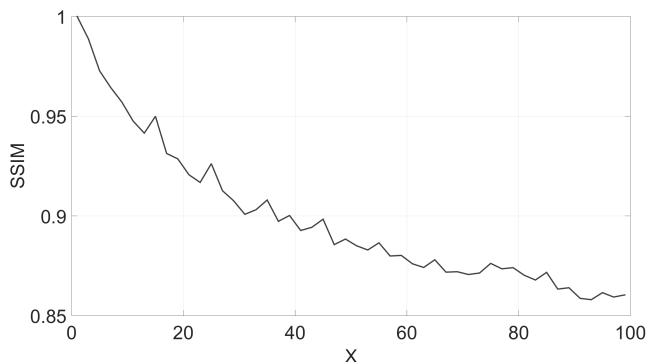


Fig. 6: Structural similarity index metric (SSIM) for varying decoding interval X .

visual quality allow for high-performant video classification with the proposed CNN-based architectures.

B. Datasets used for Video Classification

Evaluation is performed on two standard action recognition datasets, UCF-101 [30] and HMDB-51 [31]. UCF-101 is a popular action recognition dataset, comprising 13K videos from 101 action categories with 320×240 pixels per frame, at replay rate of 25 frames per second (FPS). HMDB-51 is a considerably smaller dataset, comprising only 7K videos from 51 action categories, with the same spatial resolution as UCF-101, and at 30 FPS replay rate. Finally, unless stated otherwise, we always cross-validate on the standard three splits for both datasets.

C. Evaluation Protocol and Results

For each dataset we follow the testing protocol of Section IV-D. Each UCF-101 training split consists of approximately 9.5K videos, whereas each HMDB training split has 3.7K videos. We report all single stream feedforward network runtimes without I/O, in order to isolate the efficiency of our proposed architecture. Speed is reported in terms of FPS, which is computed as the number of videos each network can process per second multiplied by the average number of frames

per video (we use the average length of UCF-101 videos, i.e., 180 frames [4]). By using FPS as our metric, we account for both the network complexity and the number of inputs processed per video at inference, i.e., the number of crops and volumes taken, as reported in the respective papers. For frameworks where the number of inputs is a function of the video size, we again assume an average video length of 180 frames. All speed results correspond to a batch size of 32 on an AWS EC2 p2.xlarge instance, which comprises a single K80 GPU.

TABLE III: Classification accuracy and speed (FPS) against state-of-the-art flow based networks. “Proposed 3D CNN” refers to our temporal stream that ingests MB motion vectors.

Framework	Input Size	Accuracy (%)		FPS
		UCF	HMDB	
Proposed 3D CNN	$24^2 \times 2 \times 160$	77.2	48.0	3105
TSCNN-Brox [4]	$224^2 \times 20$	81.2	55.4	185
LTC-Brox [5]	$58^2 \times 2 \times 100$	82.6	56.7	<100
LTC-Mpegflow [5]	$58^2 \times 2 \times 60$	63.8	–	<100
TSCNN-FlowNet2 [25]	$224^2 \times 20$	79.5	–	185
EMV-CNN (ST+TI) [6]	$224^2 \times 20$	79.3	–	1537

1) *Temporal Stream*: Table III presents the results of temporal stream CNNs on split 1 of the datasets, for which our method achieves 77.2% and 48.0% on UCF-101 and HMDB-51, respectively. When cross-validating on all three splits for both datasets, our accuracy is higher and we achieve 77.5% on UCF-101 and 49.5% on HMDB-51. It is evident that our approach performs competitively to recent proposals utilizing highly-complex optical flow, whilst minimizing the network complexity via the low number of activations in the lower convolutional layers and small spatial size of the input. As a consequence of the lower resolution inputs and longer temporal extents, our proposal is able to achieve 2 to 30-fold higher FPS in comparison to all other frameworks⁴.

The closest competitor is the MV based EMV-CNN method [6], which achieves approximately half the FPS of our approach and therefore warrants further discussion. During test-time, EMV-CNN stacks 10 P or B frames as input to their temporal stream, whereas we stack 160 P-frames per input to our 3D CNN. According to the GOP structure, for every P-frame, EMV-CNN must additionally extract and process 2 B-frames, whereas our 160 P-frame temporal extent typically constitutes processing the entire video in one forward-pass. As such, we only require 12 inputs (2 volumes, 6 crops per volume) to classify a video from UCF-101, whereas EMV-CNN evaluates on 25 inputs per video. Importantly, unlike our approach, EMV-CNN requires optical-flow based training with teacher initialization and supervision transfer from the optical flow based training [6]. This has the following detriments:

- It makes any gains stemming from codec MVs negligible during training and limits the scale-up of training.

⁴We remark that Laptev *et al.* [19] made a proposal that uses codec MVs; their method is based on the encoding of such MVs into Fisher vectors (instead of CNNs) to classify video activity. However, that approach is only capable of achieving an accuracy of 46.7% on HMDB [19] at a much lower frame rate (130 FPS) compared to recent CNN methods.

TABLE IV: Complexity of proposed 3D CNN vs EMV-CNN with respect to millions of activations and weights (#A, #W), summed over conv, pool and FC layers in the utilized deep CNN of each approach.

Framework	Complexity	
	#A($\times 10^6$)	#W($\times 10^6$)
Proposed 3D CNN	4.0	29.4
EMV-CNN [6]	2.0	90.6

- It requires upsampled P and B-frame MV fields due to the supervision transfer, which leads to reduced MV extraction and CNN processing speed in comparison to our proposal.

In order to go into more detail on the complexity of our CNN against the one proposed within EMV-CNN, we present their network complexity in Table IV. The EMV-CNN architecture requires (approximately) 3 times the number of weights (and thus 3 times the memory) of our 3D CNN.

Finally, as discussed in Section IV-D, due to the low resolution of our input, taking a large number of crops is redundant in our proposal. Therefore, it should be possible to achieve similar performance even in the case of with one-shot recognition. Indeed, when evaluating our temporal stream on a single center crop, we achieve 76.2% on UCF-101 (split 1) and 46.7% on HMDB-51 (split 1). Such a simplification increases the frame rate to 7452 FPS.

2) *Spatial Stream*: With regards to the spatial RGB stream produced by the proposed selective decoding, Table V presents results with two values of X . The network is evaluated and accuracy is subsequently averaged over cross-validation with the three splits for both datasets. The first result ($X = 10$) fully decodes every 10 frames, whilst the second result corresponds to selective decoding and rendering every 10 frames and full decoding every 50 frames. In the latter case, we set the rendering frame interval to $R = 10$ and threshold $A = 0$, i.e., selectively decoding and writing the RGB texture of macroblocks corresponding to non-zero motion vectors once every 10 frames. As the number of crops/volumes that the network evaluates on is fixed and independent of the fully decoding interval X and rendering frame interval R , the network FPS reported in Table V is the same for both cases. However, the decoding runtime for $X = 50$ is approximately 1.7 times faster than for $X = 10$ (see Table II). The results demonstrate that the performance drop from selective decoding is marginal and that our spatial stream proposal significantly outperforms TSCNN [4] and SFCNN [14] on UCF-101, whilst performing inference with approximately 5 times higher speed. We achieve this speed by restricting the inputs to single frames and only evaluating on 10 inputs per video, which counterbalances the higher complexity of our pretrained VGG16 network. On the contrary, approaches like LTC [5], TSCNN [4] and C3D [15] evaluate on many more frames and multiple crops per frame, thereby incurring higher computational overhead and significantly lower frame rate for their evaluation process. However, it is worth noting that when comparing our proposed temporal and spatial stream FPS, the

TABLE V: Classification accuracy and runtime (FPS) against state-of-the-art RGB based networks. For our proposed spatial streams, we fully decode one frame every X frames.

Framework	Input Size	Accuracy (%)		FPS
		UCF	HMDB	
Proposed, $X = 10$	$224^2 \times 3$	79.3	42.4	1228
Proposed, $X = 50$	$224^2 \times 3$	77.7	39.6	1228
TSCNN [4]	$224^2 \times 3$	73.0	40.5	252
SFCNN [14]	$170^2 \times 3 \times 10$	65.4	–	216
LTC [5]	$71^2 \times 3 \times 100$	82.4	–	<100
C3D [15]	$112^2 \times 3 \times 16$	82.3	–	<300

temporal stream runs approximately 2.5 times faster, which further motivates training the streams independently, as we can easily allocate more resources to processing the slower stream.

TABLE VI: Comparison against state-of-the-art fusion based frameworks. For our proposed two stream networks, the spatial stream ingests one fully-decoded RGB frame every X frames.

Framework	Accuracy (%)	
	UCF	HMDB
Proposed, $X = 10$	89.8	56.0
Proposed, $X = 50$	88.9	54.6
TSCNN (avg. fusion) [4]	86.9	58.0
TSCNN (SVM fusion) [4]	88.0	59.4
CNN-pool [27]	88.2	–
C3D (3 nets)+IDT [15]	90.4	–
LTC [5]	91.7	64.8
EMV + RGB-CNN [6]	86.4	–
IP+SVM [21]	–	59.5
Line Pooling [22]	88.9	62.2
TDD [37]	90.3	63.2

3) *Spatio-temporal stream fusion and complementarity in predictions*: Table VI presents the summary of the classification performance of our proposed two-stream approach (averaged over the standard three splits) when fusing the spatial and temporal streams. Our two-stream network utilizing selective decoding achieves 89.8% accuracy on UCF-101. Overall, our approach is within a few percentile points from the best results reported for both datasets, whilst skipping the complex preprocessing inherent with decoding and optical flow based methods. TSCNN, LTC and Line Pooling all use Brox optical flow in their temporal streams, whilst IP+SVM uses a combination of optical flow, pixel values and gradients for descriptor computation. On the other hand, methods such as C3D+IDT and Line Pooling use trajectory-based descriptor computation in their fusion based frameworks, in addition to deep CNN computation, which adds even further complexity to the classification pipeline. Line Pooling also adopts VGG-16 in their spatial stream as in our case, but forgoes our simpler end-to-end approach for frame pooling and VLAD encoding on an intermediate convolutional layer, which requires additional codebook learning.

Given that our spatio-temporal stream fusion strategy in-

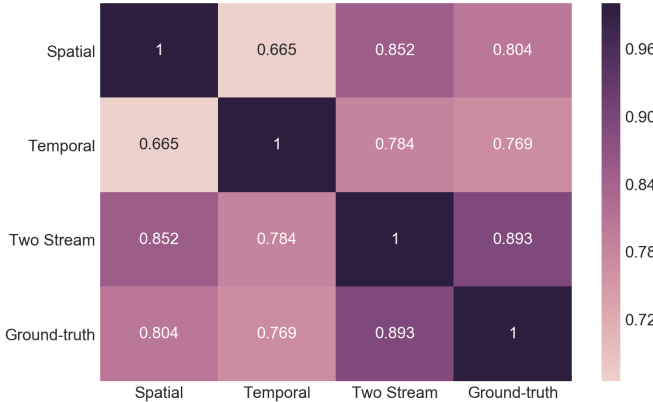


Fig. 7: Cohen’s kappa matrix over all rater combinations for UCF-101 (split 1). For the spatial stream, $X = 10$, $R = 10$.

increases the accuracy by 8%-12% in comparison to independent stream evaluation, further investigation of the inference properties of the spatial and temporal CNNs is warranted. The temporal stream ingests inputs of low spatial resolution with long temporal extent, whereas the spatial stream ingests inputs with high spatial resolution but low temporal resolution (single frames). As such, the temporal and spatial stream raters are expected to be more disjoint in their learned representations, which translates to higher information gain and a significant increase in accuracy when their inferences are fused. To quantify their pairwise agreement, we compute Cohen’s kappa κ [38] between the raters producing labels for the: temporal stream, spatial stream, two-stream and the ground truth (i.e., “null” model)

$$\kappa = \frac{p_o - p_e}{1 - p_e} \quad (1)$$

where p_o is the relative observed agreement amongst raters (equivalent to accuracy) and p_e is a hypothetical probability of random agreement, which is summation of marginal probabilities multiplied between raters. Cohen’s kappa ranges from $\kappa = 1.0$ (raters of in complete agreement) to $\kappa \leq 0$ (no agreement amongst raters other than random expectation). We plot the symmetric matrix of κ values over all rater combinations for predictions on UCF-101 (split 1) in Fig. 7. As expected, there is high inter-rater agreement between the spatio-temporal two-stream architecture and the ground-truth, with $\kappa(\text{two-stream, ground-truth}) = 0.893$. However, there is low inter-rater agreement between the independent spatial and temporal streams, i.e., $\kappa(\text{spatial, temporal}) = 0.665$. This shows that the temporal and spatial streams learn heterogenous representations that reliably classify different video subsets from the dataset. Indeed, if these video subsets were very similar to each other, then $\kappa(\text{spatial, temporal})$ would be approximately equal to $\min(\kappa(\text{spatial, ground-truth}), \kappa(\text{temporal, ground-truth})) = 0.769$; however, this is approximately 10% higher than the actual value of $\kappa(\text{spatial, temporal})$ and also turns out to be the average gain obtained by the spatio-temporal fusion.

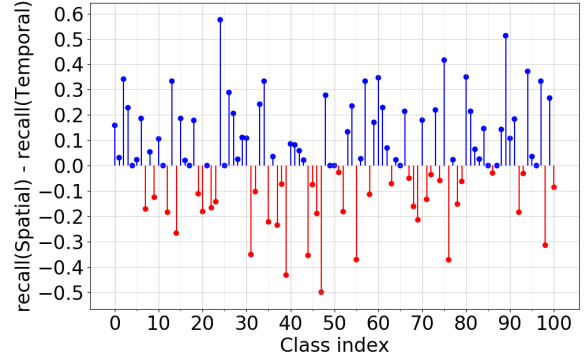


Fig. 8: Recall difference graph for UCF-101 (split 1). Red line equates to a temporal bias, blue line equates to spatial bias. Classes are in alphabetical order.

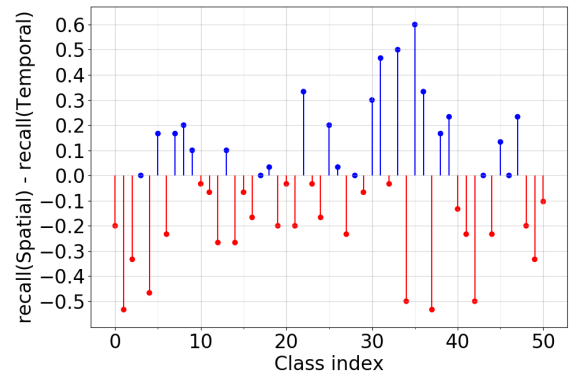


Fig. 9: Recall difference graph for HMDB-51 (split 1). Red line equates to a temporal bias, blue line equates to spatial bias. Classes are in alphabetical order.

In order to reinforce this point, we measure the difference in recall values for each class between the spatial and temporal stream, and plot this in Fig. 8 and Fig. 9 for UCF-101 and HMDB-51 respectively. If the two streams are in complete agreement, one would expect the recall difference to be close to 0; in other words, the two streams agree on the same video subsets. However, what we observe is that the temporal and spatial streams exhibit distinct biases in terms of class, depending on the nature of the activity. For UCF-101, the temporal stream is favorable for “high activity” classes, such as “high jump” (class 39), “jump rope” (class 47) and “salsa spin” (class 76). Conversely, the spatial stream performs better for “low activity” classes where a scene representation is more informative, such as “cutting in kitchen” (class 24), “rowing” (class 75) and “table tennis shot” (class 89). Intuitively, this means the stream fusion provides better generalization over all classes, or a lower network variance.

Finally, in order to associate our implementation results with the cost incurred by the two fastest methods of Table VI, namely TSCNN (avg. fusion) and EMV + RGB-CNN, we present the AWS deployment cost of each method in

TABLE VII: Cost per component and end-to-end cost C_{tot} for our proposed two-stream framework versus competitive frameworks to perform inference on UCF-101 (split 1).

Framework	C_{flow} (\$)	C_{decode} (\$)	$C_{\text{t-stream}}$ (\$)	$C_{\text{s-stream}}$ (\$)	C_{tot} (\$)
Proposed, $X = 10$	0.003	0.053	0.055	0.139	0.250
Proposed, $X = 50$	0.003	0.031	0.055	0.139	0.228
TSCNN (fusion) [4]	9.133	0.375	0.920	0.676	11.103
EMV + RGB-CNN [6]	0.006	0.375	0.111	0.676	1.167

Table VII. The table shows the cost incurred per component of each method, as well as the total end-to-end cost, C_{tot} . The four components benchmarked in the table are: flow estimation, decoding, temporal stream inference and spatial stream inference, with costs:

$$C_{\text{component}} = \frac{A}{3600} \times \frac{P_{\text{component}}}{F_{\text{component}}}, \quad (2)$$

where: A is the average number of frames required for inference in UCF-101 split 1 (180 frames/video \times 3783 videos in split 1), $F_{\text{component}}$ comprises the FPS results reported in Tables I-V for component $\in \{\text{flow, decode, t-stream, s-stream}\}$ of each method, and $P_{\text{component}}$ is the \$/hr cost of the AWS instance used to achieve the reported FPS. Specifically, based on the on-demand cost for a p2.xlarge (K80 GPU instance) and r3.xlarge (quadcore CPU) instance:

- $P_{\text{t-stream}} = P_{\text{s-stream}} = 0.9$ \$/hr and $P_{\text{decode}} = 0.333$ \$/hr,
- $P_{\text{flow}} = 0.333$ \$/hr for our proposal and EMV-CNN,
- $P_{\text{flow}} = 0.9$ \$/hr for TSCNN because it requires GPU-based Brox flow estimation.

The total cost C_{tot} to process the UCF-101 (split 1) is:

$$C_{\text{tot}} = C_{\text{flow}} + C_{\text{decode}} + C_{\text{t-stream}} + C_{\text{s-stream}}. \quad (3)$$

From Table VII, it is evident that the cost of dense optical flow in TSCNN completely overshadows all other costs. On the other hand, our MV flow incurs less than 0.005% its cost. In addition, the combination of:

- selective decoding (that incurs only 8.3% the cost of full frame decoding with $X = 50$),
- the more efficient CNN processing, and
- the cost C_{flow} of our MV flow estimation being approximately half that of EMV + RGB-CNN due to our temporal CNN only requiring 24×24 crops of the P-frame MV field (while EMV-CNN ingests upsampled P and B-frame MV fields to carry out the supervision transfer [6]),

lead to the proposed method incurring only 20% of the cost of EMV + RGB-CNN for inference. Overall, our approach is found to be 5 to 49 times cheaper to deploy on AWS than the most efficient methods from the state-of-the-art in video classification.

VI. CONCLUSION

We propose a 3D CNN architecture for video classification that utilizes compressed-domain motion vector information for substantial gains in speed and implementation cost on public cloud platforms. We fuse the 3D CNN with a spatial stream that ingests selectively decoded frames, determined by

motion vector activity. Our MV extraction is found to be three orders of magnitude faster than optical flow methods. In addition, the selective macroblock RGB decoding is one order of magnitude faster than full-frame decoding. By coupling the high MV extraction and selective RGB decoding speed with lightweight CNN processing, we are able to classify videos with one to two orders of magnitude lower cloud computing cost in comparison to the most efficient proposals from the literature, whilst maintaining competitive classification accuracy (Tables VI and VII). Further refinements of our approach may allow for the first time CNN-based classification of exascale-level video collections to take place via commodity hardware, something that currently remains unattainable by all CNN-based video classification methods that base their training on full-frame video decoding and optical flow estimation. Source code related to the proposed approach is available online, at <http://www.github.com/mvcnn>.

REFERENCES

- [1] Y. LeCun, Y. Bengio, and G. Hinton, "Deep learning," *Nature*, vol. 521, no. 7553, pp. 436–444, 2015.
- [2] C. Posch, R. Benosman, and R. Etienne-Cummings, "Giving machines humanlike eyes," *IEEE Spectrum*, vol. 52, no. 12, pp. 44–49, 2015.
- [3] C. Tan, S. Lallec, and G. Orchard, "Benchmarking neuromorphic vision: lessons learnt from computer vision," *Front. Neurosci.*, vol. 9, p. 374, 2015.
- [4] K. Simonyan and A. Zisserman, "Two-stream convolutional networks for action recognition in videos," in *Proc. Advances in Neural Inf. Process. Syst. (NIPS)*, 2014, pp. 568–576.
- [5] G. Varol, I. Laptev, and C. Schmid, "Long-term temporal convolutions for action recognition," *IEEE Trans. Patt. Anal. Mach. Intel.*, to appear.
- [6] B. Zhang *et al.*, "Real-time action recognition with enhanced motion vector CNNs," in *Proc. IEEE Conf. Comp. Vis. Pattern Rec. (CVPR)*, 2016, pp. 2718–2726.
- [7] C. Szegedy, W. Liu, Y. Jia, P. Sermanet, S. Reed, D. Anguelov, D. Erhan, V. Vanhoucke, and A. Rabinovich, "Going deeper with convolutions," in *Proc. IEEE Conf. Comp. Vis. Pattern Rec. (CVPR)*, 2015, pp. 1–9.
- [8] T. Wiegand, G. J. Sullivan, G. Bjontegaard, and A. Luthra, "Overview of the H.264/AVC video coding standard," *IEEE Trans. Circ. and Syst. for Video Technol.*, vol. 13, no. 7, pp. 560–576, 2003.
- [9] G. J. Sullivan, J. Ohm, W.-J. Han, and T. Wiegand, "Overview of the high efficiency video coding HEVC standard," *IEEE Trans. Circ. and Syst. for Video Technol.*, vol. 22, no. 12, pp. 1649–1668, 2012.
- [10] D. Mukherjee, J. Bankoski, A. Grange, J. Han, J. Koleszar, P. Wilkins, Y. Xu, and R. Bultje, "The latest open-source video codec vp9—an overview and preliminary results," in *Picture Coding Symposium (PCS)*, 2013. IEEE, 2013, pp. 390–393.
- [11] A. Krizhevsky, I. Sutskever, and G. E. Hinton, "ImageNet classification with deep convolutional neural networks," in *Proc. Advances in Neural Inf. Process. Syst. (NIPS)*, 2012, pp. 1097–1105.
- [12] H. Wang, A. Kläser, C. Schmid, and C.-L. Liu, "Action recognition by dense trajectories," in *Proc. IEEE Conf. Comp. Vis. Pattern Rec. (CVPR)*. IEEE, 2011, pp. 3169–3176.
- [13] H. Wang and C. Schmid, "Action recognition with improved trajectories," in *Proc. IEEE Int. Conf. Comput. Vis. (ICCV)*, 2013, pp. 3551–3558.

- [14] A. Karpathy *et al.*, “Large-scale video classification with convolutional neural networks,” in *Proc. IEEE Conf. Comp. Vis. Pattern Rec. (CVPR)*, 2014, pp. 1725–1732.
- [15] D. Tran, L. Bourdev, R. Fergus, L. Torresani, and M. Paluri, “Learning spatiotemporal features with 3D convolutional networks,” in *Proc. IEEE Int. Conf. Comput. Vis. (ICCV)*, 2015, pp. 4489–4497.
- [16] K. Simonyan and A. Zisserman, “Very deep convolutional networks for large-scale image recognition,” *Proc. Int. Conf. Learn. Repr. (ICLR)*, 2015.
- [17] T. Brox, A. Bruhn, N. Papenberg, and J. Weickert, “High accuracy optical flow estimation based on a theory for warping,” in *Proc. Europ. Conf. on Comp. Vis. (ECCV)*. Springer, 2004, pp. 25–36.
- [18] L. Zhao, Z. He, W. Cao, and D. Zhao, “Real-time moving object segmentation and classification from HEVC compressed surveillance video,” *IEEE Trans. on Circ. and Syst. for Video Technol.*, to appear.
- [19] V. Kantorov and I. Laptev, “Efficient feature extraction, encoding and classification for action recognition,” in *Proc. IEEE Conf. Comp. Vis. Pattern Rec. (CVPR)*, 2014, pp. 2593–2600.
- [20] A. Chadha, A. Abbas, and Y. Andreopoulos, “Compressed-domain video classification with deep neural networks: “there’s way too much information to decode the matrix,”” in *Proc. IEEE Int. Conf. on Image Process. (ICIP)*, 2017, to appear.
- [21] K. Xu, X. Jiang, and T. Sun, “Two-stream dictionary learning architecture for action recognition,” *IEEE Trans. on Circ. and Syst. for Video Technol.*, vol. 27, no. 3, pp. 567–576, 2017.
- [22] S. Zhao, Y. Liu, Y. Han, R. Hong, Q. Hu, and Q. Tian, “Pooling the convolutional layers in deep convnets for video action recognition,” *IEEE Trans. on Circ. and Syst. for Video Technol.*, to appear.
- [23] C. Feichtenhofer, A. Pinz, and A. Zisserman, “Convolutional two-stream network fusion for video action recognition,” in *Proc. IEEE Conf. Comp. Vis. Pattern Rec. (CVPR)*, 2016, pp. 1933–1941.
- [24] R. Girdhar, D. Ramanan, A. Gupta, J. Sivic, and B. Russell, “Actionvlad: Learning spatio-temporal aggregation for action classification,” *arXiv preprint arXiv:1704.02895*, 2017.
- [25] E. Ilg, N. Mayer, T. Saikia, M. Keuper, A. Dosovitskiy, and T. Brox, “FlowNet 2.0: Evolution of optical flow estimation with deep networks,” *Proc. IEEE Conf. Comp. Vis. Pattern Rec. (CVPR)*, 2017.
- [26] J. Donahue, L. Anne Hendricks, S. Guadarrama, M. Rohrbach, S. Venugopalan, K. Saenko, and T. Darrell, “Long-term recurrent convolutional networks for visual recognition and description,” in *Proc. IEEE Conf. Comp. Vis. Pattern Rec. (CVPR)*, 2015, pp. 2625–2634.
- [27] J. Yue-Hei Ng, M. Hausknecht, S. Vijayanarasimhan, O. Vinyals, R. Monga, and G. Toderici, “Beyond short snippets: Deep networks for video classification,” in *Proc. IEEE Conf. Comp. Vis. Pattern Rec. (CVPR)*, 2015, pp. 4694–4702.
- [28] M. T. Coimbra and M. Davies, “Approximating optical flow within the MPEG-2 compressed domain,” *IEEE Trans. Circ. and Syst. for Video Technol.*, vol. 15, no. 1, pp. 103–107, 2005.
- [29] “FFMPEG LibAVCodec documentation,” *online, available at: <http://ffmpeg.org/libavcodec.html>*.
- [30] K. Soomro, A. R. Zamir, and M. Shah, “UCF101: A dataset of 101 human actions classes from videos in the wild,” *arXiv preprint arXiv:1212.0402 and CRCV-TR-12-01*, Nov. 2012.
- [31] H. Kuehne *et al.*, “HMDB: a large video database for human motion recognition,” in *Proc. IEEE Int. Conf. Comput. Vis. (ICCV)*. IEEE, 2011, pp. 2556–2563.
- [32] J. Deng *et al.*, “ImageNet: A large-scale hierarchical image database,” in *Proc. IEEE Conf. Comp. Vis. Pattern Rec. (CVPR)*. IEEE, 2009, pp. 248–255.
- [33] K. He, X. Zhang, S. Ren, and J. Sun, “Delving deep into rectifiers: Surpassing human-level performance on ImageNet classification,” in *Proc. IEEE Int. Conf. Comput. Vis. (ICCV)*, 2015, pp. 1026–1034.
- [34] M. D. Zeiler and R. Fergus, “Visualizing and understanding convolutional networks,” in *Proc. Europ. Conf. on Comp. Vis. (ECCV)*. Springer, 2014, pp. 818–833.
- [35] T. Brox and J. Malik, “Large displacement optical flow: descriptor matching in variational motion estimation,” *IEEE Trans. Patt. Anal. Mach. Intell.*, vol. 33, no. 3, pp. 500–513, 2011.
- [36] Z. Wang, A. C. Bovik, H. R. Sheikh, and E. P. Simoncelli, “Image quality assessment: from error visibility to structural similarity,” *IEEE Trans. Image Process.*, vol. 13, no. 4, pp. 600–612, 2004.
- [37] L. Wang, Y. Qiao, and X. Tang, “Action recognition with trajectory-pooled deep-convolutional descriptors,” in *Proceedings of the IEEE conference on computer vision and pattern recognition*, 2015, pp. 4305–4314.
- [38] J. Cohen, “A coefficient of agreement for nominal scales,” *Educational and psychological measurement*, vol. 20, no. 1, pp. 37–46, 1960.